Journal of Power Sources 201 (2012) 376–381

Contents lists available at SciVerse ScienceDirect

Journal of Power Sources

journal homepage: www.elsevier.com/locate/jpowsour

Preparation and capacitance performance of Ag–graphene based nanocomposite

Lu Zheng[a,b], Gaini Zhang[a,b], Miao Zhang[a,b], Shaohua Guo[a,b], Zong-Huai Liu[a,b,*]

[a] Key Laboratory of Applied Surface and Colloid Chemistry (Shaanxi Normal University), Ministry of Education, Xi'an, 710062, PR China
[b] School of Materials Science and Engineering, Shaanxi Normal University, Xi'an, 710062, PR China

ARTICLE INFO

Article history:
Received 6 August 2011
Received in revised form 5 November 2011
Accepted 9 November 2011
Available online 18 November 2011

Keywords:
Graphene
Ag nanoparticles
Nanocomposite
Capacitance
Electrochemical property

ABSTRACT

Ag–graphene nanocomposite has been prepared by a simple way in situ simultaneous reduction of Ag^+ ions and graphite oxide in a solution of hydrazine hydrate at 95 °C for 12 h. The morphology and structure of the obtained material are examined by XRD, SEM, TEM, FT-IR, and XPS. The Ag nanoparticles with an average particle size of 20 nm are decorated on the surface of graphene in uniform and regular stacks, while the graphene nanosheets exist as an exfoliation state in Ag–graphene nanocomposite. The tremendous intensity decrease of the C–O and C=O XPS peaks and the disappearance of FT-IR band around 1730 cm^{-1} for Ag–graphene nanocomposite suggest that the graphite oxide has been reduced into graphene. Electrochemical properties are characterized by cyclic voltammetry and electrochemical impedance spectroscopy in 2.0 mol L^{-1} KNO_3 electrolyte. Ag–graphene nanocomposite electrode shows a characteristic Faradic capacitance behavior, and the specific capacitance value is 220 F g^{-1} at a scan rate of 10 mV s^{-1}, which is much higher than that of the graphene electrode (140 F g^{-1}). The high capacitance is ascribed to the large pseudocapacitance from the residual C–O and C=O function groups, high electrical conductivity, and less aggregation of the graphene nanosheets due to the existence of Ag particles.

1. Introduction

Graphene is a counterpart of graphite with well separated 2-D aromatic sheets composed of sp^2-bonded carbon atoms [1]. The thinner material in universe has shown many fascinating properties owing to the characteristics such as high mechanical strength, large specific surface area, high thermal stability, good electrical conductivities and excellent antibacterial activity [2–5]. Graphene can be obtained by many methods such as mechanical exfoliation of bulk graphite [6], epitaxial chemical vapor deposition on substrates [7] and chemical vapor deposition starting from carbon precursors [8]. Although the graphene with the thickness control can be prepared by these methods, the large-scale preparation of the graphene is less effective.

In terms of the yield and cost for graphene, the solution-phase preparation technique shows the most attention in recent years. In general, the solution-phase preparation technique mainly consists of two steps. Firstly, graphite is oxidized into graphite oxide with hydrophilic, and it can generate stable and homogenous colloidal suspension in aqueous solution [9]. Secondly, the graphite oxide is reduced by some reductants to remove most of the oxygen-containing groups [10]. Through the two step methods, Ruoff group has prepared thin graphene-based sheets material with a high specific surface area at 100 °C for 24 h [11], and Srinivas group has prepared a graphene-based powder material with highly agglomerated and disordered sheets and high surface area of 640 m^2 g^{-1} at 80 °C for 24 h [12]. During the solution-phase preparation process of graphene, a challenge question is how to avoid the aggregation reaction of graphene nanosheets and obtain the graphene with high individual dispersion. Although the aggregation reaction of the graphene nanosheets can be reduced through the intercalation of other molecules or ions into the interlayer, the electronic properties of the obtained materials such as the resistance are obviously influenced [13–15].

In order to reduce the aggregation reaction of the graphene nanosheets and obtain the graphene with good electrical conductivity and high individual dispersion, some inorganic nanoparticals, such as metals or semiconductors have been intercalated into the interlayer of the graphene nanosheets [16–18]. The obtained graphene–metal nanocomposites show promising applications in fields of chemical sensors [19], optical and electronic devices [20], and energy storage [21], etc. Ag nanoparticles, as good metal conductor, show many novel physical, chemical and catalytic properties [22]. If Ag nanoparticles are introduced into the interlayer of the graphene nanosheets, the obtained nanocomposite is respected

* Corresponding author at: School of Materials Science and Engineering, Shaanxi Normal University, Xi'an, Shaanxi, 710062, China. Tel.: +86 29 85303701; fax: +86 29 85307774.
E-mail address: zhliu@snnu.edu.cn (Z. Liu).

0378-7753/$ – see front matter © 2011 Elsevier B.V. All rights reserved.
doi:10.1016/j.jpowsour.2011.11.026

to have not only good dispersion, but also good conductivity. Recently, several groups have obtained graphene–Ag nanocomposite with favorable properties. Pasricha group has prepared graphene–Ag nanosheet materials with good conductivity in two steps [23]. Liu group has prepared the Ag nanoparticles wrapping around 1D carbon materials by an environmentally benign and a simple method with the assistance of supercritical carbon dioxide [24]. Ye group has prepared the graphene–Ag nanohybrid by a solution-based approach involving the chemical reduction of silver ions in chemically converted graphene suspensions with mixed reducing agents [25]. Yang group has prepared graphene–Ag nanocomposite through a solvothermal method using ethylene glycol or DI water/hydrazine as solvent and reducing agent [26]. Although Ag–graphene nanocomposites with different properties have been prepared by the above groups, the preparation methods are long-time cost. Meanwhile, the capacitance performance of the obtained material is not investigated. In the present work, Ag–graphene nanocomposite was prepared by a simple way in situ simultaneous reduction of Ag^+ ions and graphite oxide, and its capacitance performance was also discussed.

2. Experimental

2.1. Materials

Crude flake graphite (carbon content: 99.9%) was purchased from Qingdao Aoke Co., China. Hydrazine hydrate (50%), $AgNO_3$ and KNO_3 were obtained from Sinopharm Chemical Reagent Co., Ltd., China, in analytical purity and used without further purification. Deionized water was used throughout the experiments.

2.2. Preparation of Ag–graphene nanocomposite

Graphite oxide (GO) was prepared from natural graphite powder through a modified Hummers method [27]. 0.1 g GO was dispersed in 100 mL H_2O and stirred overnight to form a homogeneous aqueous dispersion. Then 100 mL $AgNO_3$ solution (0.02 mol L^{-1}) was added into the GO dispersion, and the obtained suspension was treated by ultrasonic treatment (600 W, 80% amplitude) for 1 h and followed by stirring at room temperature for 12 h. The suspension was separated by centrifugation, and the obtained sediment was washed with deionized water for several times. Ag^+ ions intercalated GO was finally obtained after the sediment was freeze-dried for 24 h, which was abbreviated as Ag^+–GO. Ag^+–GO material (200 mg) was soaked in 200 ml deionized water, and hydrazine hydrate (200 (L) was then added into the dispersion. The obtained mixture was stirred for 30 min and heated at 95 °C for 12 h, the yellow–brown suspension gradually changed into black precipitate. After separated by centrifugation, the black sediment was washed with water, and the freeze-dried material was Ag–graphene nanocomposite, which was abbreviated as Ag–RGO. Meanwhile, to compare with the above experimental results, the graphene (RGO) material was prepared in the same way from GO dispersion without Ag^+ ions.

2.3. Characterizations

X-ray diffraction (XRD) measurements were carried out by using a D/Max-3c X-ray diffractometer with Cu Kα (λ = 1.5406 Å), with an operation voltage and current of 40 kV and 40 mA, respectively. A Quanta 200 environmental scanning electron microscopy (SEM) was used to observe the morphology of the obtained samples. Transmission electron microscopy (TEM) images were collected by using a JEM-2100 microscope at 200 kV. Specimens for observation were prepared by dispersing the samples into alcohol by ultrasonic treatment and dropped on carbon–copper grids. X-ray photoelectron spectroscopy (XPS) was performed on a K-ALPHA with an Al cathode as the X-ray source at a power of 150 W (accelerating voltage 12 kV, current 6 mA) in a vacuum of 8.0×10^{-8} mPa. Fourier transform infrared (FT-IR) spectra were recorded by a Nicolet AVATAR 360 FTIR spectrometer.

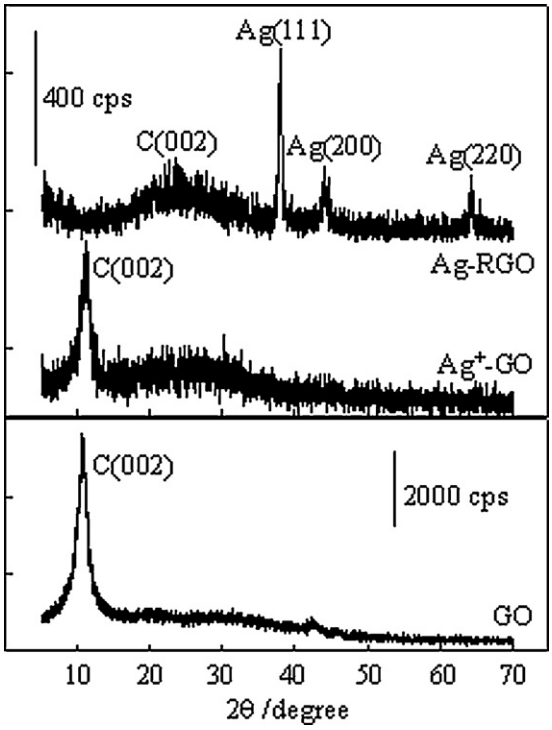

Fig. 1. XRD patterns of samples obtained at different stages.

Electrochemical measurement: The electrochemical performances of the as-obtained material electrodes were tested using a cyclic voltammetry (CV) method and electrochemical impedance spectroscopy (EIS) with a three-electrode electrochemical setup. The working electrode was prepared by mixing sample (90 wt.%) as active material with polyvinylidene fluoride (10 wt.%). Polyvinylidene fluoride was used as binder, and it was firstly dissolved with acetone. The two materials were mixed together to obtain a rubber-like paste which was brush-coated onto a Ni foam. The foam was dried at 110 °C in air for 2 h to remove the solvent. After drying, the coated foam was uniaxially pressed to completely adhere to the electrode material with the current collector. The thickness, the area and the coated loading of the working electrode were 0.5 mm, 2.01 cm^2 and 0.0048 g cm^{-2}, respectively. Platinum foil (2 cm^2) and a saturated calomel electrode (SCE) were used as the counter and reference electrodes, respectively [28]. The cyclic voltammetry measurement was carried out between −0.2 and 0.8 V and the specific capacitance was evaluated from the area of the charge and discharge curve of the CV plot [29]. The electrochemical impedance measurement was performed after the electrodes reached the end of discharge and relaxed until the open circuit potential reached 0.1 V. The measurements were taken over a series of cycles in a frequency range of 100 kHz to 0.1 Hz with AC amplitude of 10 mV. All electrochemical measurements were carried out by using Ivium-Stat electrochemical workstation (Ivium Technologies BV, Holland) in 2 mol L^{-1} KNO_3 aqueous solution at room temperature.

3. Results and discussion

The XRD patterns of the precursor GO, Ag^+–GO, and Ag–RGO nanocomposite are shown in Fig. 1. GO has a layered structure with a basal spacing of 0.73 nm, showing the complete oxidation of

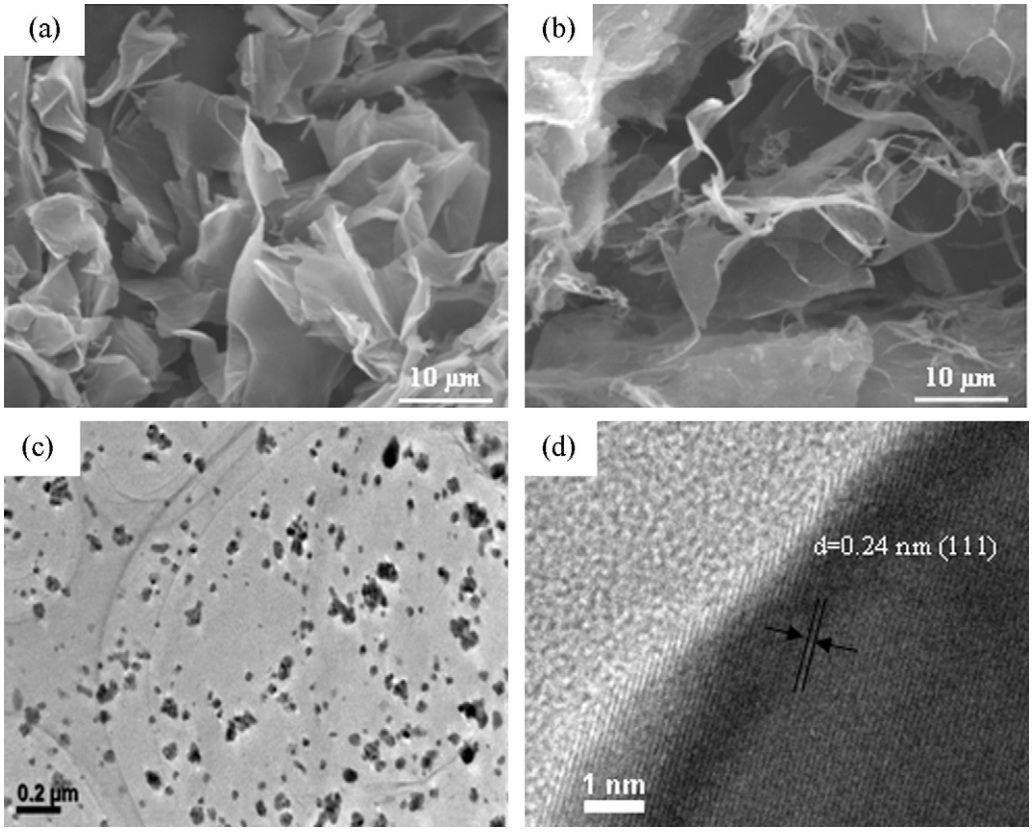

Fig. 2. SEM images of samples GO (a) and Ag–RGO nanocomposite (b), TEM image (c) and HRTEM image (d) of Ag–RGO nanocomposite.

graphite into the graphite oxide [9]. The basal spacing is larger than the origin graphite (0.33 nm), indicating that the interlayer distance is remarkably expanded during the chemical oxidation. After GO is reacted with 0.02 M $AgNO_3$ solution at room temperature for 12 h, the basal spacing slightly increases to 0.76 nm for sample Ag^+–GO. These results show that Ag^+ ions are intercalated into the interlayer of the precursor GO, and the layered structure of GO is maintained. On the other hand, sample Ag^+–GO is soaked in hydrazine hydrate (200 (L) and followed by heating at 95 °C for 12 h, the XRD pattern of Ag–RGO nanocomposite obviously changes. Some characteristic peaks at 37.9°, 44.1°, 64.5° with high intensity are corresponding with the (1 1 1), (2 0 0) and (2 2 0) planes of the cubic Ag crystal (JCPDS No. 04-0783), which indicate that the metallic Ag nanoparticles are formed after being reduced. However, the characteristic peak at 10.6° which corresponds to (0 0 2) plane of GO disappears, while the characteristic peak at 24.1° which corresponds to (0 0 2) plane of graphene is slightly observed. These results suggest that a simultaneous reduction process of Ag^+ ions and GO is carried out when sample Ag^+–GO is treated in hydrazine hydrate and followed by heating, and Ag–RGO nanocomposite is successfully prepared. On the other hand, the (0 0 2) plane peak of RGO becomes broad and its intensity becomes weak, indicating that the Ag nanoparticles are decorated on the surface of RGO in uniform and regular stacks and the graphene nanosheets exist in an exfoliation state in Ag–RGO nanocomposite [30,31]. Recent studies have shown that the diffraction peaks become weak or even disappear if the regular stacks of graphite oxide or graphite are destroyed, for example by exfoliation [32]. It does not matter whether the existence state of the carbon sheets is graphite oxide or graphene in these composites, but it is confirmed that the regular layered structure of graphite oxide or graphene is destroyed. Because of the low weight content of Ag nanoparticles in the obtained nanocomposite (about 12.2%), the influence of the as-reduced metals on the XRD patterns of graphite or graphite oxide is not considerable [33]. While the metallic salts are added to the above system, the carbon sheets easily aggregate and then deposit. A possible explanation is that the adsorption of the as-reduced Ag nanoparticles on the surface results in the formation of heavier entities, consequently leading to a quick sedimentation. The attached particles may also prevent the restacking of these graphene nanosheets, therefore, the characteristic diffraction peaks of the layered structure disappear.

SEM image shows that precursor GO has a thin sheet with a thickness less than 0.5 μm (Fig. 2a). In comparison with the precursor GO, an ultrathin nanosheet flaky morphology can be observed from Ag–RGO nanocomposite (Fig. 2b). The representative SEM image shows randomly dispersed, thin, crumpled sheets closely associated with each other and forming a highly exfoliated bundle [34]. The TEM image shows that graphene nanosheets are decorated by Ag nanoparticles with an average particle size of 20 nm (Fig. 2c). In the present work, the oxygen-containing groups on GO sheets supply the chemical active centers for Ag deposition, and thus Ag nanoparticles are well separated with each other and distributed randomly on the graphene nanosheets. Although the Ag nanoparticles are irregular and well separated, some bigger Ag particles with size of >50 nm are still observed, indicating some agglomeration behavior of smaller Ag nanoparticles. Fig. 2d is the high-resolution image of sample Ag–RGO nanocomposite, the measured lattice fringe spacing in the image is about 0.24 nm, which agrees well with the (1 1 1) crystal plane of Ag nanoparticles [35].

The X-ray photoelectron spectroscopy (XPS) spectrum can be used to observe the inner structure of C for carbon-based materials. The XPS results indicate that a decrease tendency of the oxygen content is carried out in the obtained materials. As shown in Fig. 3a, the intensity of some oxygenated functional groups on carbon sheets in the as-synthesized composites is obviously reduced, indicating the change of carbon content. It is well known

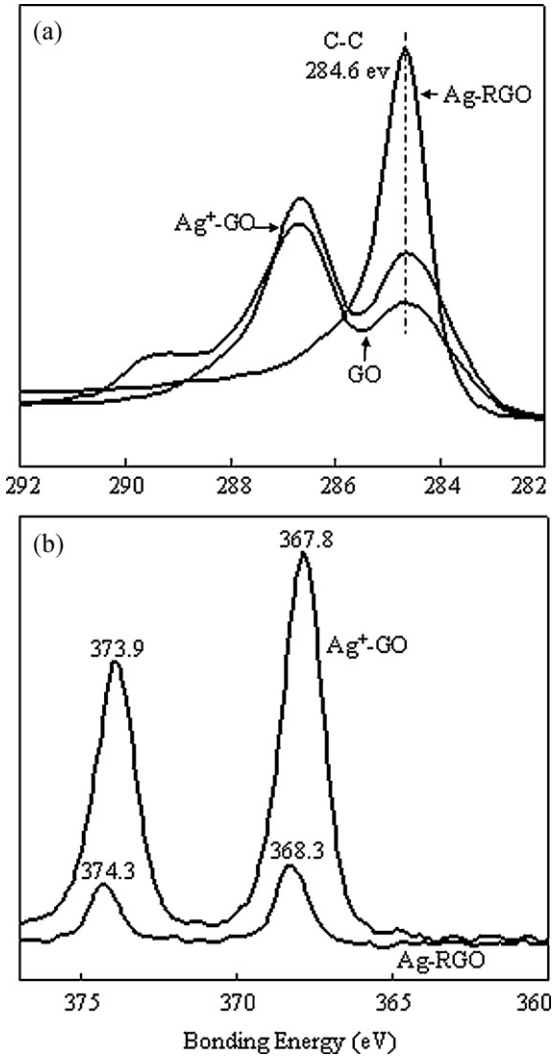

Fig. 3. C1s XPS spectra of GO, Ag^+–GO and Ag–RGO nanocomposite (a) and Ag 3d XPS spectra of Ag^+–GO and Ag–RGO nanocomposite (b).

that the bands centered at 284.6 eV and 372.8 eV are associated with C1s and Ag 3d, respectively. The XPS spectrum for each sample can be deconvoluted into four peaks, corresponding to carbon atoms in four functional groups: carbon sp^2 (C–C, 284.6 eV), epoxy/hydroxyls (C–O, 286.2 eV), carbonyl (C═O, 287.8 eV), and carboxylates (O═C–O, 289.0 eV) (Supporting information Fig. S1). For the precursor GO, the four peaks of C1s spectrum corresponding to the functional groups: carbon sp^2, epoxy/hydroxyls, carbonyl, and carboxylates can be observed, suggesting that graphite has been completely oxidized into GO [26]. The peak intensity of C–O and C═O is still strong in Ag^+–GO material, showing that oxygenated functional groups still exist in this material. In contrast, the peak intensity of C–O and C═O significantly decreases and the content of C–C sharply increases after the reduction process, suggesting that the oxygen-containing of graphene oxide is removed. Meanwhile, the two peaks around at 367.8 eV and 373.9 eV corresponding to Ag 3d5/2 and 3d3/2 binding energies for Ag^+–GO material are shifted to higher energies (368.3 eV and 374.3 eV) in Ag–RGO nanocomposite due to the change of the chemical environment. These results indicate that Ag valence still maintain 1+ in Ag^+–GO material, while Ag nanoparticles are existed in Ag–RGO nanocomposite [36,37].

The as-obtained GO, Ag^+–GO, and Ag–RGO nanocomposite are further analyzed by means of FTIR spectroscopy and the results

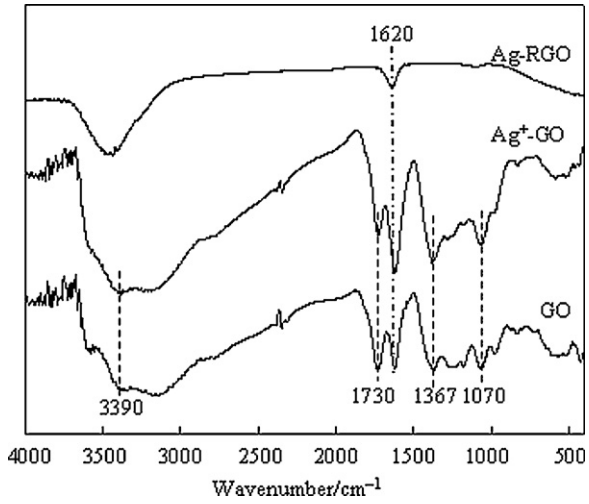

Fig. 4. FT-IR spectra of samples obtained at different stages.

are shown in Fig. 4. As seen from the spectra of GO and Ag^+–GO, the band at 3390 cm^{-1} arises from the –OH stretching vibration. There are also bands due to carboxyl C═O and C–C groups (1730 and 1620 cm^{-1}), epoxy C–O (1367 cm^{-1}), and alkoxy C–O (1070 cm^{-1}) groups situated at the edges of the GO nanosheets, as previously reported [38]. After the reduction treatment, most of the absorption bands are absent leaving mainly the absorption band of C–C vibration (around 1620 cm^{-1}) in the spectrum of Ag–RGO nanocomposite. The peak loss at 3390 cm^{-1} confirms the involvement and reduction of oxygen-containing groups in the formation of Ag nanoparticles. Besides, it also suggests that strong interactions may exist between the Ag nanoparticles and the remaining surface hydroxyl O atoms [25].

Cyclic voltammetry is considered to be an ideal tool for the electrochemical property characterization of the cathode material. The electrochemical behavior of the obtained RGO and Ag–RGO nanocomposite is investigated using three-electrode cell between −0.2 and 0.8 V in a KNO_3 electrolyte at a sweep rate of 10 mV s^{-1} and the results are shown in Fig. 5. For RGO electrode material, the cyclic voltammetric curve is relatively rectangular in shape and exhibits near mirror-image current response on voltage reversal, indicating an obvious supercapacitive behavior for the RGO electrode. Meanwhile, the curve shows no peak, indicating that the electrode capacitor is charged and discharged at a pseudoconstant rate over the complete voltammetric cycle [39,40]. The specific capacitance

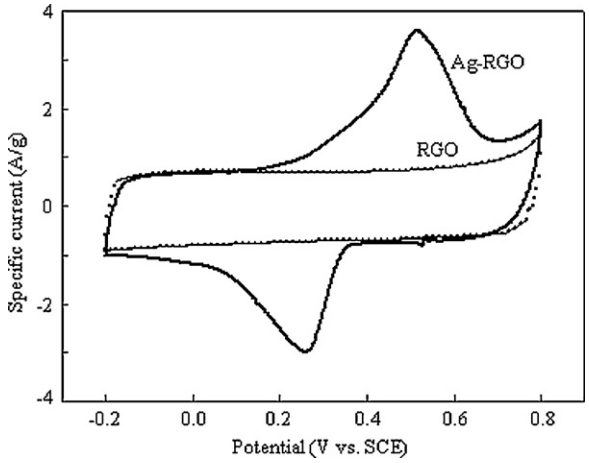

Fig. 5. The CV curves of RGO and Ag–RGO nanocomposite electrodes at 10 mV s^{-1} in 2.0 mol L^{-1} KNO_3 electrolyte in the voltage range −0.20–0.80 V vs. SCE.

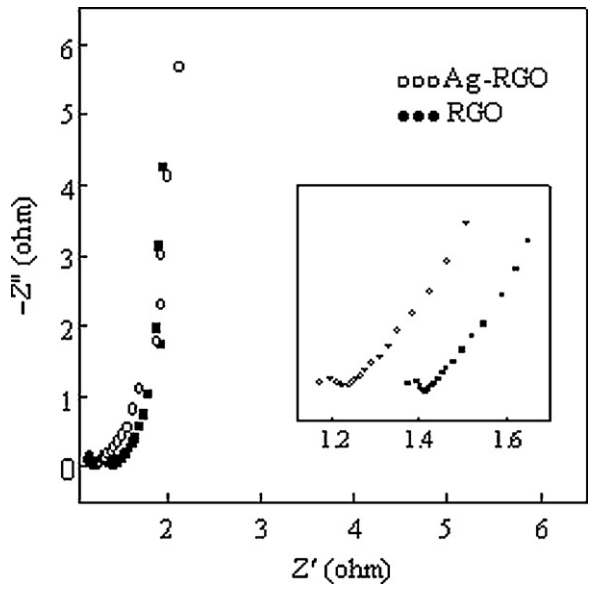

Fig. 6. The Nyquist plots of RGO and Ag–RGO nanocomposite electrodes with a frequent range of 0.1 Hz–10 kHz in 2.0 mol L^{-1} KNO_3 electrolyte.

value calculated from the CV curve is found to be 140 F g^{-1}. On the other hand, the CV curve of Ag–RGO nanocomposite electrode is very different from that of RGO electrode under the same condition. A pair of well-separated redox peaks (anodic peak at 0.51 V, with corresponding cathodic peak at 0.26 V) is observed, indicating that the measured capacitance is based on the redox mechanism. However, the redox peaks are not only broad but also asymmetric, indicating that the redox peaks correspond to the multi redox couples. The broad and asymmetric redox peaks are probably caused by the multi oxidation of both Ag and the residual C–O and C=O function groups. The experimental results of the electrodes and electrolytes obtained after 10 cycles and 400 cycles of charge processes show that Ag nanoparticles are hardly oxidized Ag(I), and Ag(I) ions are too little to be detected after 10 cycles, while some Ag nanoparticles are oxidized to Ag(I) after 400 cycles. Therefore, Ag^+ ions oxidized might be trapped in RGO, and they could be detected by XPS for the electrode. In addition, the broad redox peaks arising from the redox reactions of surface functionalities become weaker and finally diminish at higher scan rates, due to the relatively slow charge/discharge kinetic [41]. For Ag–RGO electrode, the CV curve shows relatively mirror image with respect to the zero-current line, announcing that the obtained cathode has excellent capacitive property. In comparison with the specific capacitance of RGO electrode, the specific capacitance of Ag–RGO nanocomposite electrode is 220 F g^{-1}. The high capacitance is ascribed to the large pseudocapacitance from the residual C–O and C=O function groups, high electrical conductivity, and less aggregation of the graphene nanosheets due to the existence of Ag nanoparticles.

The electrochemical impedance can be used to understand the resistance characteristic of RGO and Ag–RGO nanocomposite. The Nyquist plots of RGO and Ag–RGO nanocomposite are shown in Fig. 6. The Nyquist plots of the two materials in 2.0 mol L^{-1} KNO_3 electrolyte are similar to each other in shape, consisting of a semicircle in the high frequency range and a straight line in the low frequency range. The semicircle at high frequency range is due to the charge transfer reaction at the interface of the electrolyte/oxide electrode; and it corresponds to the charge transfer resistance (R_{ct}) and it can be calculated by extrapolation of the semicircle on the real impedance axis [39]. The diameter of the semicircles has a decrease tendency in an order of Ag–RGO > RGO, indicating that the R_{ct} of Ag–RGO electrode is smaller than that of RGO and the electrochemical reaction on the electrode/electrolyte interface is the most facile. This result confirms that the presence of Ag nanoparticles indeed decreases the electronic resistivity of the electrode. In addition, the inclined line in low frequency range is attributable to Warburg impedance resulting from the frequency dependence of ion diffusion and transport in the electrolyte [42]. It can be seen that the linear region of the plot exhibits an angle relative to the real axis, and the angle relative to the real axis increases in the order of Ag–RGO > RGO electrode with the decrease of frequency. Meanwhile, the value of the intercept at the real axis in the high frequency range can be used to estimate the sum of resistances arising from the electrolyte, the intrinsic resistance of the active material, and the contact resistance between the active material and the current collector (R_Ω). R_Ω of Ag–RGO cathode is 1.1 Ω, which is lower than that of 1.3 Ω for RGO electrode. These results show that the addition of Ag nanoparticles onto RGO electrode can significantly improve the electrical performance due to the intrinsic resistance change of the active material and less aggregation of the graphene nanosheets.

4. Conclusion

A simple simultaneous reduction method of Ag^+ ions and GO in a solution of hydrazine hydrate has been developed to prepare Ag–RGO hybrid nanocomposite. The Ag nanoparticles with an average particle size of 20 nm are decorated on the surface of RGO in uniform and regular stacks and the graphene nanosheets exist in an exfoliation state in Ag–RGO nanocomposite. The residual C–O and C=O function groups lead to large pseudocapacitance, and the existence of Ag nanoparticles prevents the aggregation of the graphene nanosheets. The high capacitance for Ag–RGO electrode material (220 F g^{-1}) is ascribed to the large pseudocapacitance, less aggregation, and relatively slow charge/discharge kinetic. The Ag–RGO nanocomposite is a promising electrode for energy storage/conversion device with excellent performance.

Acknowledgements

This work was supported by the National Natural Science Foundation of China (20971082 and 51172137), the Natural Science Key Foundation of Shaanxi Province (2011JZ001), Changjiang Scholars and Innovative Research Team in University (IRT1070) and the Fundamental Research Funds for the Central Universities (GK200901002 and GK201001001).

Appendix A. Supplementary data

Supplementary data associated with this article can be found, in the online version, at doi:10.1016/j.jpowsour.2011.11.026.

References

[1] K. Novoselov, A. Geim, S. Morozov, D. Jiang, Y. Zhang, S. Dubonos, I. Grigorieva, A. Firsov, Science 306 (2004) 666–669.
[2] K. Kim, H.-J. Park, B. Woo, K. Kim, G. Kim, W.-S. Yun, Nano Lett. 8 (2008) 3092–3096.
[3] C. Lee, X.-D. Wei, J. Kysar, J. Hone, Science 321 (2008) 385388.
[4] C. Rao, A. Sood, K. Subrahmanyam, A. Govindaraj, Angew. Chem., Int. Ed. 48 (2009) 7752–7777.
[5] W. Lv, D.-M. Tang, Y.-B. He, C.-H. You, Z.-Q. Shi, X.-C. Chen, C.-M. Chen, P.-X. Hou, C. Liu, Q.-H. Yang, ACS Nano 3 (2009) 3730–3736.
[6] J.-M. Michael, J.-L. Li, Chem. Mater. 19 (2007) 4396–4404.
[7] K. Kim, Y. Zhao, H. Jang, S. Lee, J. Kim, K. Kim, J. Ahn, P. Kim, J. Choi, B.-H. Hong, Nature 457 (2009) 706–710.
[8] Y. Shi, K. Kim, A. Reina, M. Hofmann, L.-J. Li, J. Kong, ACS Nano 4 (2010) 2689–2694.
[9] R. Daniel, S. Park, C. Bielawski, R. Ruoff, Chem. Soc. Rev. 39 (2010) 228–240.

[10] Y. Zhou, Q.-L. Bao, L.-L. Tang, Y.-L. Zhong, K. Loh, Chem. Mater. 21 (2009) 2950–2956.
[11] S. Stankovich, D. Dikin, R. Piner, K. Kohlhaas, A. Kleinhammes, Y.-Y. Jia, Y. Wu, S. Nguyen, R. Ruoff, Carbon 45 (2007) 1558–1565.
[12] G. Srinivas, Y.-W. Zhu, R. Piner, N. Skipper, M. Ellerby, R. Ruoff, Carbon 48 (2010) 630–635.
[13] H. Bai, C. Li, G.-Q. Shi, Adv. Mater. 23 (2011) 1089–1115.
[14] R. Kou, Y.-Y. Shao, D.-H. Mei, Z.-M. Nie, D.-H. Wang, C.-M. Wang, V. Viswanathan, S. Park, I. Aksay, Y.-H. Lin, Y. Wang, J. Liu, J. Am. Chem. Soc. 133 (2011) 2541–2547.
[15] V. Prashant, J. Phys. Chem. Lett. 1 (2010) 520–527.
[16] M. Ryan, S. Brian, V. Prashant, J. Phys. Chem. C 112 (2008) 5263–5266.
[17] M. GilGoncalves, C. Granadeiro, H. Nogueira, M. Singh, J. Gracio, Chem. Mater. 21 (2009) 4796–4802.
[18] Q. Cheng, J. Tang, J. Ma, H. Zhang, N. Shinya, L.-C. Qin, Carbon 49 (2011) 2917–2925.
[19] W.-J. Hong, H. Bai, Y.-X. Xu, Z.-Y. Yao, Z.-Z. Gu, G.-Q. Shi, J. Phys. Chem. C 114 (2010) 1822–1826.
[20] S. Liu, J.-Q. Tian, L. Wang, H.-L. Li, Y.-W. Zhang, X.-P. Sun, Macromolecules 43 (2010) 10078–10083.
[21] Y.-C. Si, E. Samulski, Chem. Mater. 20 (2008) 6792–6797.
[22] S. Solomon, M. Bahadory, A. Jeyarajasingam, S. Rutkowsky, C. Boritz, J. Chem. Educ. 84 (2007) 322–325.
[23] R. Pasricha, S. Gupta, A. Srivastava, Small 5 (2009) 2253–2259.
[24] A. Niu, Y.-J. Han, J. Wu, N. Yu, Q. Xu, J. Phys. Chem. C 114 (2010) 12728–12735.
[25] J.-F. Shen, M. Shi, N. Li, B. Yan, H.-W. Ma, Y.-Z. Hu, M.-X. Ye, Nano Res. 3 (2010) 339–349.
[26] H.-W. Tien, Y.-L. Huang, S.-Y. Yang, J.-Y. Wang, C.-C. Ma, Carbon 49 (2011) 1550–1560.
[27] W. Hummers, R. Offeman, J. Am. Chem. Soc. 80 (1958) 1339.
[28] V. Subramanian, H. Zhu, B. Wei, J. Power Sources 159 (2006) 361–364.
[29] C.-Z. Yuan, B. Gao, X.-G. Zhang, J. Power Sources 173 (2007) 606–612.
[30] C. Xu, X. Wang, J. Zhu, J. Phys. Chem. C 112 (2008) 19841–19845.
[31] D.-Y. Cai, M. Song, J. Mater. Chem. 17 (2007) 3678–3680.
[32] T. Szabo, O. Berkesi, P. Forgo, K. Josepovits, Y. Sanakis, D. Petridis, I. Dekany, Chem. Mater. 18 (2006) 2740–2749.
[33] Y.-C. Xing, J. Phys. Chem. B 108 (2004) 19255–19259.
[34] N. Timothy, A. Carlos, H. Bernadette, L. Ping, S. Nelson, A. Andrea, F. Thomas, J. Timothy, R. David, L. Dale, J. Phys. Chem. C 113 (2009) 19812–19823.
[35] F.-L. Li, J.-F. Song, H.-F. Yang, S.-Y. Gan, Q.-X. Zhang, D.-X. Han, A. Ivaska, L. Niu, Nanotechnology 20 (2009) 455–602.
[36] Q. Xiang, G.-F. Meng, Y. Zhang, J.-Q. Xu, P.-C. Xu, Q.-Y. Pan, W.-J. Yu, Sens. Actuators B 143 (2010) 635–640.
[37] T. Kaspar, T. Droubay, S. Chambers, P. Bagus, J. Phys. Chem. C 114 (2010) 21562–21571.
[38] T. Kuilla, S. Bhadra, D.-H. Yao, N. Kim, S. Bose, J. Lee, Science 35 (2010) 1350–1375.
[39] Y. Wang, Z.-Q. Shi, Y. Huang, Y.-F. Ma, C.-Y. Wang, M.-M. Chen, Y.-S. Chen, J. Phys. Chem. C 113 (2009) 13103–13107.
[40] L.-L. Zhang, X.-S. Zhao, Chem. Soc. Rev. 38 (2009) 2520–2531.
[41] Z. Lin, Y. Liu, Y. Yao, O. Hildreth, Z. Li, K. Moon, C.-P. Wong, J. Phys. Chem. C 115 (2011) 7120–7125.
[42] Y.-J. Guo, S.-J. Guo, J.-T. Ren, Y.-M. Zhai, S.-J. Dong, E. Wang, ACS Nano 4 (2010) 4001–4010.